Proceedings of the

17th International Modal Analysis Conference

FEBRUARY 8-11, 1999
HYATT ORLANDO HOTEL
KISSIMMEE, FLORIDA

TECHNICAL PROGRAM CHAIR:
Alfred L. Wicks, Virginia Polytechnic Institute and State University
Dominick J. DeMichele, Honorary Technical Chair

SOCIETY FOR EXPERIMENTAL MECHANICS, INC.:
Kristin L. MacDonald, Executive Director
Katherine M. Ramsay, Conference Manager

Organized By:

SOCIETY FOR EXPERIMENTAL MECHANICS, INC.
Bethel, Connecticut 06801

29. Non-linear Systems

30. Modal Analysis Applied to Bridge Assessment

Developed by: H. Ghasemi, Turner-Fairbank Highway Research Center

Nonlinear Identification of a Scaled Structural Dynamic Model of the F-15 Tail Section

Ayman A. El-Badawy and **Ali H. Nayfeh**

Department of Mechanical Engineering
Department of Engineering Science and Mechanics
Virginia Polytechnic Institute and State University
Blacksburg, VA 24061, USA

ABSTRACT

The present study is concerned with the nonlinear identification of a structural dynamic model of the twin-tail assembly of the F-15 fighter plane. It is modeled with two coupled nonlinear-ordinary differential equations. Experimental modal analysis is used to identify the linear natural frequencies and associated damping ratios of the two tails separately. Then, the model is excited by a principal parametric resonance. The experimental results are combined with a perturbation solution to identify the nonlinear stiffness and damping of each tail separately. Finally, a combination of a perturbation method and the nonlinear dynamic response of the full model is used to identify the linear coupling of the two tails. Predictions of the identified mathematical model are qualitatively in agreement with the experimentally obtained force and frequency-response curves.

NOMENCLATURE

$i = 1, 2$	pertaining to the right and left tail respectively
t	time
$u_i(t)$	generalized coordinates of the motion of the tail
ω_i	natural frequencies
Ω	driving frequency
σ_i	detunings that describe the nearness of Ω to ω_i
η_i	transmissibility terms
α_i	coefficients of the cubic nonlinearity of the tails
μ_i	viscous damping coefficients of the tails
μ_3, μ_4	aerodynamic damping coefficients of the tails
k	coupling coefficient of the twin tails
τ_i	arbitrary phase angles
u_{ij}	terms in the expansion of u(t)
T_0	fast time scale
T_1	slow time scale
F	amplitude of the excitation force
D_{ij}	partial derivative with respect to T_j
ϵ	small bookkeeping parameter
$a_i(T_1)$	amplitude of the motion of the tails
$\gamma_i(T_1)$	phase lag between the input and output
p_i, q_i	coefficients in the frequency response equation

1 INTRODUCTION

Present combat aircraft require agility and high maneuvering at high angles of attack. In this flight regime, an induced buffeting flow occurs when the airflow on the upper wing surface becomes detached. This buffeting flow will induce high-frequency oscillations of the twin vertical tails in fighter aircraft, such as the F-15 and F-18. Alleviation of buffeting is critical for extending the service life of the tail section. The purpose of this paper is to develop a scheme for the nonlinear identification of the linear and nonlinear dynamical characteristics of the F-15 aircraft twin-tail structure. The model can then be used to develop control strategies for buffet alleviation.

A complete understanding of the tail buffet loads and the tail responses will eventually lead to the ability of predicting and alleviating buffeting. We use nonlinear identification techniques to estimate the nonlinear parameters in a mathematical model of the tail assembly. Nayfeh et al [1] proposed a consistent methodology whereby perturbation techniques, complex Fourier amplitudes, and higher-order statistics can be combined to characterize and quantify the parameters of nonlinear systems. They used the method to identify the parameters of a three-beam two-mass frame. Fahey and Nayfeh [2] estimated the nonlinear parameters by regressive fits. We extend these techniques to the F-15 tail section.

2 MODELLING

The tail section used in the experiments is a 1/16 dynamically scaled model of the F-15 tail assembly. The model was constructed by Professor Sathya Hanagud of the Georgia Institute

of Technology from a series of aluminum channels, brass rings, composite plates, metal masses, and various adhesives, as shown in Figure 1. The model is approximately 0.355 *m* long, 0.228 *m* tall, and 0.482 *m* wide. The objective of this work is to develop a mathematical model that can capture the dynamics of the twin-tail assembly and identify its linear and nonlinear parameters. We use a combination of experimental modal analysis, nonlinear vibration testing, and perturbation methods.

For the nonlinear vibration testing, we mount the model on a 250-lb shaker and excite it with a principal parameter resonance. The tail deflections are measured with a series of four Micromeasurments Group CEA-06-125UW-350 strain gages. The centers of the gage pairs are 0.9 *cm* and 8.5 *cm* from the top of the aluminum channels. One pair is on the outside of the right vertical tail; the other pair is on the outside of the left vertical tail. Changes in the gages are measured with a Micromeasurments Group 2310 strain gage conditioning amplifier, in a quarter bridge configuration.

In the nonlinear identification, we exploit resonances to maximize the influence of the nonlinear parameters on the response. For the arrangement in Figure 2, the maximum response occurs when the excitation frequency is near twice the natural frequency of either of the vertical tails; that is, principal parametric resonance.

A series of bolts and several positioning blocks fixes the model to a 250-lb shaker. In this way, we are able to excite parametrically the tails without any additional masses. The shaker excitation is measured with a PCB 308 B09 accelerometer studded to the base. The accelerometer signal is conditioned with a PCB 482A10 amplifier. The shaker amplifier is driven with a Wavetek 650 signal generator. The signal from the accelerometer amplifier and the strain gage conditioner is read with a data acquisition computer using LABVIEW software. The signals sent to the data acquisition computer are conditioned with a Krohn-Hite 3905 multiple channel filter set at 100 Hz low pass. The system identification is carried out using a Hewlett Packard 3562A two-channel signal analyzer and a Tektronix 2030 oscilloscope. A PCB model 086 B01 impulse force hammer is also employed for impact testing. Figure 2 shows the experimental setup.

The experimental results show that the tails are responding in their first bending modes. Hence, the assembly is modeled with two oscillators, each describing a tail. We let u_1 and u_2 denote the generalized coordinates of the first bending modes of the two tails and let ω_1 and ω_2 be their linear undamped natural frequencies. For energy dissipation, we note that the surface areas of the tails are large and hence include both viscous damping and airflow drag. Thus, we incorporate linear and quadratic damping terms. To account for large deflections, we add a cubic nonlinear term to each oscillator. By plucking one tail, we have obtained a response in the other tail. Hence, we include linear coupling terms. They account for structural as well as aerodynamic coupling between the tails. Thus, we assume that the dynamics of the tails are governed by the following two mass-

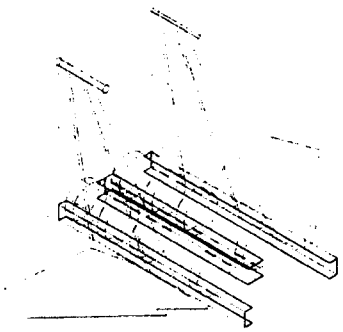

Figure 1: A three-dimensional view of the twin tails

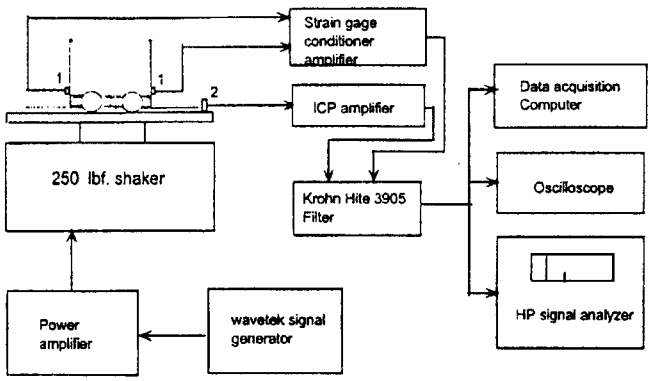

1 : MicroMeasurments Strain Gage CEA 06 125 UW 350

2 Accelerometer PCB 303A02

Figure 2: Experimental setup

normalized second-order coupled differential equations:

$$\ddot{u}_1 + \omega_1^2 u_1 = -2\mu_1 \dot{u}_1 - \alpha_1 u_1^3 - \mu_3 \dot{u}_1 \mid \dot{u}_1 \mid + k(u_2 - u_1) \quad (1)$$

$$\ddot{u}_2 + \omega_2^2 u_2 = -2\mu_2 \dot{u}_2 - \alpha_2 u_2^3 - \mu_4 \dot{u}_2 \mid \dot{u}_2 \mid + k(u_1 - u_2) \quad (2)$$

For the arrangement shown in Figure 2, we add the forcing terms $u_1 \eta_1 F \cos(\Omega t + \tau_1)$ and $u_2 \eta_2 F \cos(\Omega t + \tau_2)$ to the right hand side of Equations (1) and (2). To induce the maximum response, we let $\Omega \approx 2\omega_1, \omega_2 \approx \omega_1$.

3 IDENTIFICATION OF LINEAR TERMS

The first step in the identification of any nonlinear system is the identification of its linear parameters: natural frequencies,

damping ratios, and modal factors of the dominant modes. To accomplish this, we used experimental modal analysis. We used an impact hammer to excite the structure and then generate frequency-response functions. We averaged the transfer functions of 10 sequential hammer impacts. We consistently tried to strike the tails in the normal direction and at the same location every time. By monitoring the frequency spectrum, we chose a tip for the hammer such that the drop in the frequency spectrum of an impact was less than 10% in the frequency range of interest. To avoid leakage, we used an exponential window. We zoomed around the first natural frequency to improve the resolution and hence to better estimate the linear identified parameters. During the experiments, we periodically checked the natural frequencies to detect any fatigue damage. The hammer impacts were done very close to the strain gages to realize a collocated response.

In Figures 3 and 4, we show the average frequency-response functions (FRFs) and their coherence functions for the right and left tails, respectively. Double hits were avoided. Clearly the tails resonant peaks are fairly well separated. An antiresonance always follows a resonance, which is a characteristic of a point FRF. The coherence function drops at the antiresonances, as expected.

We used very small excitation levels to obtain the frequency-response functions shown in Figures 3 and 4. The transfer functions are sensitive to slight changes in the excitation level. The location of the first natural frequency changes with excitation level.

The experimentally determined natural frequency of the first bending mode of the right tail is 9.135 Hz and that of the left tail is 9.05 Hz. An estimate of the linear damping ratios of the tails were found using both the half-power point and the logarithmic decrement over ten periods of the oscillations of each tail. The average was used to give a damping ratio of 0.14 % for the right tail and 0.19 % for the left tail. The values obtained with both techniques were nearly equal. An alternate way of estimating the linear damping coefficients is through a nonlinear technique, as discussed in the next section.

4 IDENTIFICATION OF NONLINEAR TERMS

We used the method of multiple scales [3-5] to derive four first-order nonlinear differential equations governing the modulation of the amplitudes and phases of both tails. These equations were used to construct the steady-state amplitudes and phases as functions of the excitation amplitude and frequency. We estimated the parameters of the model from regressive fits between the experimentally and theoretically determined steady-state response amplitudes.

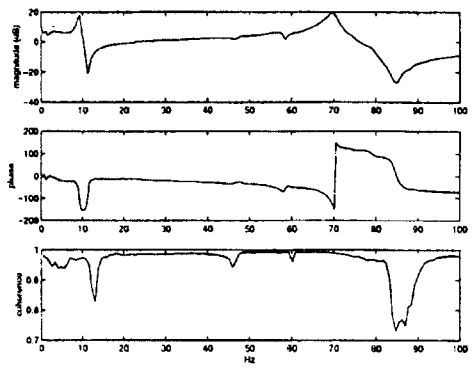

Figure 3: Frequency-response and coherence functions for the right tail

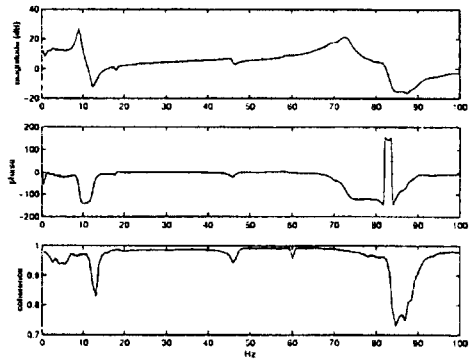

Figure 4: Frequency-response and coherence functions for the left tail

4.1 Approximate Solution

To determine an approximate solution of Equations (1) and (2), we introduce a nondimensional parameter ϵ as a bookkeeping parameter. Then, we scale the α_i, μ_i, k, and F as $\epsilon\alpha_i, \epsilon\mu_i, \epsilon k$, and ϵF. Moreover, to quantitatively describe the nearness of the resonances, we introduce the detuning parameters σ_1 and σ_2 defined by $\Omega = 2\omega_1 + \epsilon\sigma_1$ and $\omega_2 = \omega_1 + \epsilon\sigma_2$.

Using the method of multiple scales, we seek a first-order uniform expansion of the solution of Equations (1) and (2) in the form

$$u_1 = u_{11}(T_0, T_1) + \epsilon u_{12}(T_0, T_1) + \cdots \quad (3)$$

$$u_2 = u_{21}(T_0, T_1) + \epsilon u_{22}(T_0, T_1) + \cdots \quad (4)$$

where $T_0 = t$ is a fast time scale and $T_1 = \epsilon t$ is a slow time

scale. In terms of T_0 and T_1, the time derivatives become

$$\frac{d}{dt} = D_0 + \epsilon D_1 + \cdots \tag{5}$$

$$\frac{d^2}{dt^2} = D_0^2 + 2\epsilon D_0 D_1 + \cdots \tag{6}$$

where $D_n = \frac{\partial}{\partial T_n}$. Substituting Equations (3)-(6) into Equations (1) and (2) and equating coefficients of like powers of ϵ gives

$O(\epsilon^0)$:

$$D_0^2 u_{11} + \omega_1^2 u_{11} = 0 \tag{7}$$

$$D_0^2 u_{21} + \omega_2^2 u_{21} = 0 \tag{8}$$

$O(\epsilon)$:

$$\begin{aligned} D_0^2 u_{12} + \omega_1^2 u_{12} = & -2D_0 D_1 u_{11} - 2\mu_1 D_0 u_{11} + \eta_1 k_1 (u_{21} - u_{11}) \\ & -\alpha_1 u_{11}^3 - \mu_3 D_0 u_{11} \mid D_0 u_{11} \mid \\ & +\eta_1 u_{11} F \cos(\Omega t + \tau_1) \end{aligned} \tag{9}$$

$$\begin{aligned} D_0^2 u_{22} + \omega_2^2 u_{22} = & -2D_0 D_1 u_{21} - 2\mu_2 D_0 u_{21} + \eta_2 k_2 (u_{11} - u_{21}) \\ & -\alpha_2 u_{21}^3 - \mu_4 D_0 u_{21} \mid D_0 u_{21} \mid \\ & +\eta_2 u_{21} F \cos(\Omega t + \tau_2) \end{aligned} \tag{10}$$

The general solution of Equations (7) and (8) can be written as

$$u_{11} = A_1(T_1) e^{i\omega_1 T_0} + \bar{A}_1(T_1) e^{-i\omega_1 T_0} \tag{11}$$

$$u_{21} = A_2(T_1) e^{i\omega_2 T_0} + \bar{A}_2(T_1) e^{-i\omega_2 T_0} \tag{12}$$

where the $A_i(T_1)$ are determined by eliminating the secular terms from the next-order approximation.

Substituting Equations (11) and (12) into Equations (9) and (10) yields

$$\begin{aligned} D_0^2 u_{12} + \omega_1^2 u_{12} = & -2i\omega_1 (A_1' e^{i\omega_1 T_0} + 2i\omega_1 \bar{A}_1{}' e^{-i\omega_1 T_0}) \\ & -2\mu_1 i\omega_1 A_1 e^{i\omega_1 T_0} + 2\mu_1 i\omega_1 \bar{A}_1 e^{-i\omega_1 T_0} \\ & +\eta_1 k (A_2 e^{i\omega_2 T_0} + \bar{A}_2 e^{-i\omega_2 T_0} - A_1 e^{i\omega_1 T_0} \\ & -\bar{A}_1 e^{-i\omega_1 T_0}) - \alpha_1 A_1^3 e^{3i\omega_1 T_0} \\ & -3\alpha_1 A_1^2 \bar{A}_1 e^{i\omega_1 T_0} - 3\alpha_1 A_1 \bar{A}_1{}^2 e^{-i\omega_1 T_0} \\ & -\alpha_1 \bar{A}_1{}^3 e^{-3i\omega_1 T_0} - \mu_3 [(i\omega_1 A_1 e^{i\omega_1 T_0} \\ & -i\omega_1 \bar{A}_1 e^{-i\omega_1 T_0}) | i\omega_1 A_1 e^{i\omega_1 T_0} \\ & -i\omega_1 \bar{A}_1 e^{-i\omega_1 T_0} |] + \eta_1 \frac{F}{2} (A_1 e^{i\omega_1 T_0} \\ & +\bar{A}_1 e^{-i\omega_1 T_0}) (e^{i(2\omega_1 T_0 + \sigma_1 T_1 + \tau_1)} \\ & +e^{-i(2\omega_1 T_0 + \sigma_1 T_1 + \tau_1)}) \end{aligned} \tag{13}$$

$$\begin{aligned} D_0^2 u_{22} + \omega_2^2 u_{22} = & -2i\omega_2 (A_2' e^{i\omega_2 T_0} + 2i\omega_2 \bar{A}_2{}' e^{-i\omega_2 T_0}) \\ & -2\mu_2 i\omega_2 A_2 e^{i\omega_2 T_0} + 2\mu_2 i\omega_2 \bar{A}_2 e^{-i\omega_2 T_0} \\ & +\eta_2 k (A_2 e^{i\omega_2 T_0} + \bar{A}_2 e^{-i\omega_2 T_0} - A_2 e^{i\omega_2 T_0} \\ & -\bar{A}_2 e^{-i\omega_2 T_0}) - \alpha_2 A_1^3 e^{3i\omega_2 T_0} \\ & -3\alpha_2 A_2^2 \bar{A}_2 e^{i\omega_2 T_0} - 3\alpha_2 A_2 \bar{A}_2{}^2 e^{-i\omega_2 T_0} \\ & -\alpha_2 \bar{A}_2{}^3 e^{-3i\omega_2 T_0} - \mu_4 [(i\omega_2 A_2 e^{i\omega_2 T_0} \\ & -i\omega_2 \bar{A}_2 e^{-i\omega_2 T_0}) | i\omega_2 A_2 e^{i\omega_2 T_0} \\ & -i\omega_2 \bar{A}_2 e^{-i\omega_2 T_0} |] + \eta_2 \frac{F}{2} (A_2 e^{i\omega_2 T_0} \\ & +\bar{A}_2 e^{-i\omega_2 T_0}) (e^{i(2\omega_2 T_0 + \sigma_4 T_1 + \tau_2)} \\ & +e^{-i(2\omega_2 T_0 + \sigma_4 T_1 + \tau_2)}) \end{aligned} \tag{14}$$

Eliminating the terms that produce secular terms in Equations (13) and (14) gives

$$\begin{aligned} 2i\omega_1 A_1' = & -2\mu_1 i\omega_1 A_1 + \eta_1 k A_2 e^{i\sigma_2 T_1} - \eta_1 k A_1 - 3\alpha_1 A_1^2 \bar{A}_1 \\ & +\frac{1}{2}\eta_1 F \bar{A}_1 e^{i\sigma_1 T_1 + \tau_1} - i\frac{4}{3\pi}\mu_3 \omega_1^2 a_1^2 e^{i\beta_1} \end{aligned} \tag{15}$$

$$\begin{aligned} 2i\omega_2 A_2' = & -2\mu_2 i\omega_2 A_2 + \eta_2 k A_1 e^{i\sigma_3 T_1} - \eta_2 k A_2 - 3\alpha_2 A_2^2 \bar{A}_2 \\ & +\frac{1}{2}\eta_2 F \bar{A}_2 e^{i\sigma_4 T_1 + \tau_2} - i\frac{4}{3\pi}\mu_4 \omega_2^2 a_2^2 e^{i\beta_2} \end{aligned} \tag{16}$$

4.2 Equilibrium Solutions and Their Stability

To determine the stability of the solutions of Equations (15) and (16), we introduce the Cartesian transformation

$$A_k = \frac{1}{2}[p_k(T_1) - iq_k(T_1)] e^{(i\nu_k T_1 + \frac{1}{2}\tau_k)}, \quad k = 1, 2 \tag{17}$$

where

$$\nu_1 = \beta_1' = \frac{1}{2}\sigma_1 \text{ and } \nu_2 = \beta_2' = \frac{1}{2}\sigma_1 - \sigma_2 \tag{18}$$

separate real and imaginary parts, and obtain

$$\begin{aligned} p_1' = & -\nu_1 q_1 - \mu_1 p_1 - \frac{1}{2\omega_1}\eta_1 k q_2 + \frac{1}{2\omega_1}\eta_1 k q_1 + \frac{3}{8\omega_1}\alpha_1 p_1^2 q_1 \\ & +\frac{3}{8\omega_1}\alpha_1 q_1^3 + \frac{\eta_1 F}{4\omega_1} q_1 - \frac{4}{3\pi}\mu_3 \omega_1 \sqrt{p_1^2 + q_1^2}\, p_1 \end{aligned} \tag{19}$$

$$\begin{aligned} q_1' = & \nu_1 p_1 - \mu_1 q_1 + \frac{1}{2\omega_1}\eta_1 k p_2 - \frac{1}{2\omega_1}\eta_1 k p_1 - \frac{3}{8\omega_1}\alpha_1 p_1^3 \\ & -\frac{3}{8\omega_1}\alpha_1 p_1 q_1^2 + \frac{\eta_1 F}{4\omega_1} p_1 - \frac{4}{3\pi}\mu_3 \omega_1 \sqrt{p_1^2 + q_1^2}\, q_1 \end{aligned} \tag{20}$$

$$\begin{aligned} p_2' = & -\nu_2 q_2 - \mu_2 p_2 - \frac{1}{2\omega_2}\eta_2 k q_1 + \frac{1}{2\omega_2}\eta_2 k q_2 + \frac{3}{8\omega_2}\alpha_2 p_2^2 q_2 \\ & +\frac{3}{8\omega_2}\alpha_2 q_2^3 + \frac{\eta_2 F}{4\omega_2} q_2 - \frac{4}{3\pi}\mu_4 \omega_2 \sqrt{p_2^2 + q_2^2}\, p_2 \end{aligned} \tag{21}$$

$$\begin{aligned} q_2' = & \nu_2 p_2 - \mu_2 q_2 + \frac{1}{2\omega_2}\eta_2 k p_1 - \frac{1}{2\omega_2}\eta_2 k p_2 - \frac{3}{8\omega_2}\alpha_2 p_2^3 \\ & -\frac{3}{8\omega_2}\alpha_2 p_2 q_2^2 + \frac{\eta_2 F}{4\omega_2} p_2 - \frac{4}{3\pi}\mu_4 \omega_2 \sqrt{p_2^2 + q_2^2}\, q_2 \end{aligned} \tag{22}$$

We set the time derivatives in Equations (19)-(22) equal to zero and solve the resulting system of algebraic equations for

p_1, q_1, p_2 and q_2 for a specified value of either σ_1, which is a measure of the detuning of the principal parametric resonance, or F, which is a measure of the forcing amplitude. The amplitudes a_1 and a_2 of the responses of the two tails were then calculated from $a_i = \sqrt{p_i^2 + q_i^2}$. Since there is no closed-form solution for the four algebraic equations, we resorted to numerical techniques, Numerical integration of the modulation equations for different sets of initial conditions was used to locate some of the possible solutions for a given σ_1 and F. Then, starting with these solutions, we used a pseudo arclength scheme [6] to trace the branches of the equilibrium solutions by varying either σ_1 or F.

The stability of a particular equilibrium solution is determined by examining the eigenvalues of the Jacobian matrix of the right-hand sides of Equations (19)-(22). If the real part of each eigenvalue of the Jacobian matrix is negative, the corresponding equilibrium solution is asymptotically stable. If the real part of any of the eigenvalues is positive, the corresponding equilibrium solution is unstable.

4.3 Curve Fitting of Amplitude Sweeps

To identify the nonlinear parameters, we held one of the tails completely fixed, set the excitation frequency at 18 Hz, and slowly swept the excitation amplitude. The resulting force-response curve is shown in Figure 5. Then we repeated the same test for the left tail. The results are shown in Figure 6.

Mathematically, we achieve the uncoupling by setting $k = 0$ in Equations (15) and (16). Then, expressing A_1 in the polar form

$$A_1 = \frac{1}{2} a e^{i\beta} \tag{23}$$

setting $k = 0$, and separating real and imaginary parts in Equations (15), we obtain

$$a' = -\mu_1 a - \frac{4\mu_3}{3\pi}\omega_1 a^2 + \frac{\eta_1 F a}{4\omega_1}\sin\gamma \tag{24}$$

$$a\beta' = \frac{3\alpha_1}{8\omega_1}a^3 - \frac{\eta_1 F a}{4\omega_1}\cos\gamma \tag{25}$$

where

$$\gamma = \sigma_1 T_1 - 2\beta + \tau_1 \tag{26}$$

The equilibrium solutions of Equations (24)-(25) correspond to $a' = 0$ and $\gamma' = 0$. There are two possibilities: $a = 0$ and $a \neq 0$. In the latter case, the equilibrium solutions are given by

$$F\sin\gamma = \Psi a + \Gamma \tag{27}$$

$$F\cos\gamma = \Phi a^2 + \Lambda \tag{28}$$

where $\Psi = \frac{16\omega_1^2\mu_3}{3\pi\eta_1}$, $\Gamma = \frac{4\omega_1\mu_1}{\eta_1}$, $\Phi = \frac{3\alpha_1}{2\eta_1}$, and $\Lambda = -\frac{2\omega_1\sigma_1}{\eta_1}$. Equations (27) and (28) constitute four equations in the four unknowns μ_1, μ_3, α_1, and η_1. From physics, we know that the damping terms must be positive while α_1 must be negative

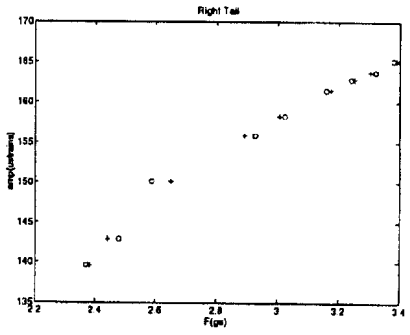

Figure 5: Least-square error fit of the experimental data for the right tail

because the tails possess a softening-type nonlinearity. These constrains are enforced in the curve-fitting algorithm.

Squaring and adding Equations (27) and (28) yields

$$F = \sqrt{\Phi^2 a^4 + (\Psi^2 + 2\Phi\Lambda)a^2 + 2\Psi\Gamma a + \Gamma^2 + \Lambda^2} \tag{29}$$

A curve-fitting algorithm that uses polynomials will not work in this case because of the radical and the absence of the cubic term. Hence, we used the MATLAB built-in function called *fmins*. To this end, we defined $c_1 = \Phi^2$, $c_2 = (\Psi^2 + 2\Phi\Lambda)$, $c_3 = 2\Psi\Gamma$, and $c_4 = \Gamma^2 + \Lambda^2$. Then, we minimized the error

$$E = \sum_{i=1}^{n}\left(F_i - \left(\sqrt{c_1 a^4 + c_2 a^2 + c_3 a + c_4}\right)_i\right)^2 \tag{30}$$

where n is the number of data points. *fmins* then returned a vector containing the coefficients that provide a local minimum near the initial guesses. Knowing the c_i allowed us to solve for Ψ, Γ, Φ, and Λ. Since the equations are nonlinear, they possess several solutions. Imposing the constrains on the signs and demanding that the orders of magnitude of the parameters be consistent with those expected, we eliminated some of these solutions. Moreover, we used the estimated linear damping coefficient as a check on that estimated with the nonlinear scheme. Finally, we determined μ_1, μ_3, α_1, and η_1.

We repeated the procedure for the left tail and identified μ_2, μ_4, α_2, and η_2.

In the experiments, we performed both amplitude and frequency sweeps. However, we only used the amplitude sweeps in the identification. The identified parameters for the right tail are $\zeta_1 = 0.01357$, $\mu_3 = 3.157 \times 10^{-4}\mu\epsilon^{-1}$, $\alpha_1 = -3.675 \times 10^{-2}\frac{1}{s^2\mu\epsilon^2}$, and $\eta_1 = 161.54\frac{1}{gs^2}$. The identified parameters are for the left tail are $\zeta_2 = 0.01856$, $\mu_4 = 1.958864 \times 10^{-4}\mu\epsilon^{-1}$, $\alpha_2 = -2.977 \times 10^{-3}\frac{1}{s^2\mu\epsilon^2}$, and $\eta_2 = 275.12\frac{1}{gs^2}$. In Figure 5, we show the experimental data and the best fit for the right tail, whereas in Figure 6, we show the experimental data and the best fit for the left tail. The agreement is excellent, as expected.

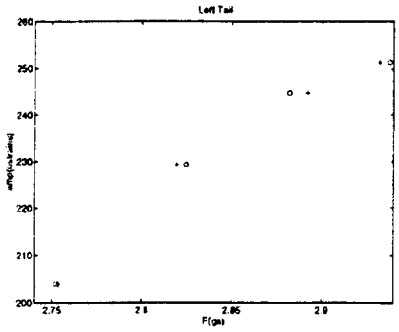

Figure 6: Least-squares error fit of the experimental data for the left tail

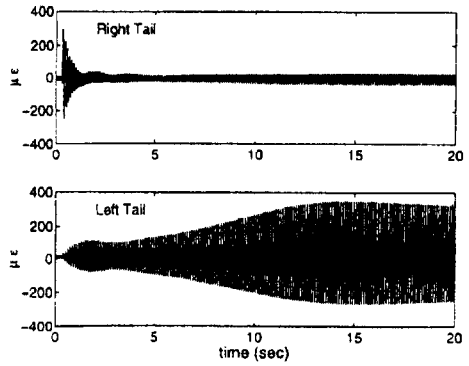

Figure 7: Energy transfer through the mechanism of one-to-one autoparametric resonance

5 IDENTIFICATION OF LINEAR COUPLING COEFFICIENT

To estimate the linear coupling coefficient k, we note from Equations (1) and (2) that it has two effects. First, the term $-ku_1$ in Equation (1) and the term $-ku_2$ shift the linear natural frequencies of the individual tails. Second, the term ku_2 in Equation (1) and the term ku_1 in Equation (2) couple the responses of the two tails. The shift in the natural frequencies is small and hence cannot be used to accurately estimate k. On the other hand, the coupling effect is very strong as described below and hence it can be used to accurately estimate k.

We fixed the excitation amplitude and varied the excitation frequency around 18 Hz. For the same excitation amplitude and frequency, we found five possible responses depending on the initial conditions: (a) very small-amplitude motions of both tails, (b) a large-amplitude motion of the right tail accompanied by a small-amplitude motion of the left tail, (c) a large-amplitude motion of the left tail accompanied by a small-amplitude motion of the right tail, (d) a large-amplitude motion involving both tails moving in phase, and (e) a large-amplitude motion involving both tails moving out-of-phase. The coexisting five responses are the result of the nonlinearities. These results point out some of the shortcomings of testing models with one rigid and one flexible tail or even testing only one tail counting on symmetry.

An interesting phenomenon was observed in the response of the scaled model. Fixing the excitation amplitude and frequency and plucking one tail, we observed that the oscillations of the plucked tail decayed with time and the unplucked tail oscillated with a large amplitude. The time traces of an example are shown in Figure 7.

By trial and error, we estimated k by comparing experimentally and theoretically obtained force-response curves. We determined force-response curves by using the experimental setup in Figure 2. We set the excitation frequency at 18 Hz and the excitation amplitude at 2.5 g. Then, we gave many disturbances to the tails, but the tails remained motionless. We incremented the excitation level and repeated the procedure. When the excitation level was increased to 2.7 g, we found two steady-state motions depending on the initial conditions: an in-phase motion and an out-of-plane motion. We picked one of these responses, recorded the time histories, and then incremented the excitation level. The procedure was repeated until the excitation level reached 3.40 g. Then, we converted the time records to the frequency domain. In Figure 8, we show an example of the excitation time history and the resulting in-phase and out-of-phase time histories as well as their corresponding spectra. We extracted the response amplitudes and plotted the results in Figure 9 for the case in which the response of the left tail is larger than that of the right tail in one case and the response of the right tail is larger than that of the left tail in another case.

Next, we guessed a value for k, used the identified $\omega_i, \alpha_i, \mu_i$, and η_i, set the excitation frequency at 18 Hz, and chose a set of initial conditions. Then, we integrated the modulation equations (19)-(22). We varied the initial conditions and the excitation amplitude F until we obtained all nontrivial solutions. Then, we used a pseudoarclength to trace the equilibrium solutions. We varied k until the experimentally and theoretically obtained force-response curves are qualitatively in agreement. In this way, we estimated a value of 87 $(1/sec^2)$ for k. The theoretically obtained force-response curves are shown in Figure 10.

CONCLUSION

We used experimental data of a 1/16 structural dynamic scale model of the F-15 aircraft to develop a mathematical model of its twin-tail assembly. The model consists of two oscillators, each of which has linear and quadratic damping terms and a cubic nonlinear term. The two oscillators are coupled linearly. Experimental modal analysis was used to estimate their linear natural frequencies, and damping ratios. The model was then

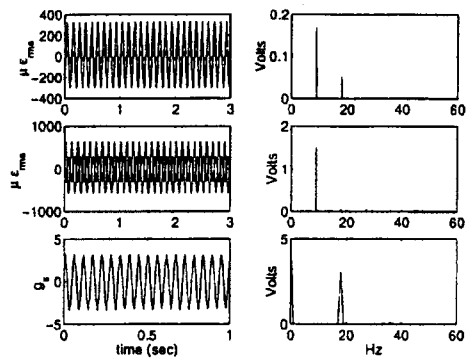

Figure 8: Examples of in-phase and out-of-phase motions and the excitation

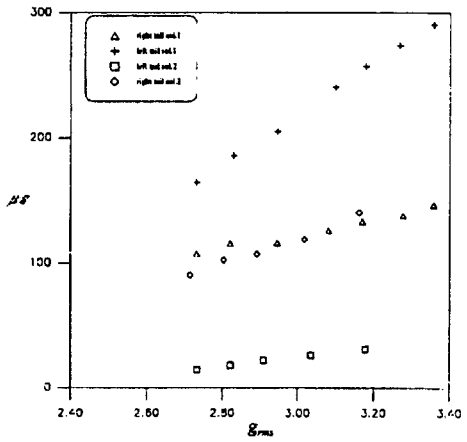

Figure 9: Experimentally obtained amplitude-response curves (left tail response is larger than that of right tail) at 18.0 Hz. (Forward Sweep)

excited by a principal parametric resonance (twice its natural frequency). The force-response curves obtained experimentally are compared with those obtained with the method of multiple scales to estimate the nonlinear parameters as well as the linear coupling parameter.

ACKNOWLEDGMENT

This work was supported by the Air Force Office of Scientific Research under Grant No. F496020-98-1-0393.

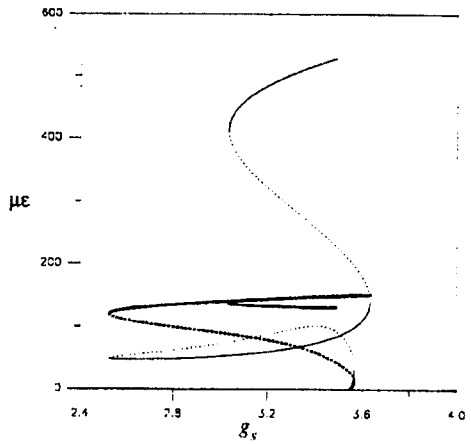

Figure 10: Theoretically obtained amplitude-response curve at 18.0 Hz when $k = 87$ $(1/sec^2)$

REFERENCES

[1] **Nayfeh, A. H., Hajj, M. R., Fung, J., & Fahey, S. O'F.**, '*Characterization and Identification of Damping and Nonlinear Systems Parameters with Bispectral Analysis*', ASME Design Engineering Technical Conferences ASME DETC97/VIB-4407, Sacramento, CA, September 14-17, 1997.

[2] **Fahey, S. O'F.**, and **Nayfeh A. H.**, '*Experimental Nonlinear Identification of a Single Structural Mode*', 16th International Modal Analysis Conference, Santa Barbara, CA, February 3-5, 1998.

[3] **Nayfeh, A. H.**, Perturbation Techniques, Wiley-Interscience, New York, 1973.

[4] **Nayfeh, A. H.**, Introduction to Perturbation Techniques, Wiley-Interscience, New York, 1981.

[5] **Nayfeh, A. H.**, and **Mook, D. T.**, Nonlinear Oscillations, Wiley-Interscience, New York, 1979.

[6] **Nayfeh, A. H.**, and **Balachandran, B.**, Applied Nonlinear Dynamics, Wiley-Interscience, New York, 1995.